JOURNAL OF PROPULSION AND POWER
Vol. 17, No. 4, July–August 2001

Combustion of Magnesium with Carbon Dioxide and Carbon Monoxide at Low Gravity

Angel Abbud-Madrid,* Abhijit Modak,† Melvyn C. Branch,‡ and John W. Daily§
University of Colorado, Boulder, Colorado 80309-0427

The burning behavior and flame structure of magnesium in pure carbon dioxide and pure carbon monoxide atmospheres in low-gravity conditions are investigated. Cylindrical specimens are suspended by a thermocouple wire and are radiatively ignited. Spherical flames are obtained during steady-state burning of the metal sample with increasing metal-oxide accumulation in an outer shell. Burning times twice as long as in normal gravity are observed, revealing a diffusion-controlled reaction. The burning time is proportional to the square of the metal sample diameter. Combustion of magnesium with carbon monoxide is not possible without constant heating of the sample. A one-dimensional, quasi-steady numerical model of the spherically symmetric diffusion flame using elementary gas-phase reactions and detailed transport property calculations shows qualitative agreement with the observed structure of the flames. It predicts a maximum temperature close to the vaporization–decomposition point of the metal oxide, as well as the coexistence of the gaseous and condensed phases of the oxide product. It also predicts a diffusion-controlled reaction for magnesium burning in oxygen, air, and carbon dioxide and provides an accurate comparison of the burning rates of these systems. The discrepancies between the numerical simulation and the experimental observations may be attributed to the absence of accurate condensation, radiation, and surface-reaction models.

Nomenclature

C_p	=	specific heat
D	=	ordinary multicomponent diffusion coefficient matrix
D^T	=	thermal diffusion (Soret effect) coefficient
d	=	diameter of sample
H_{fg}	=	latent heat
h	=	enthalpy
M	=	mass flux
R	=	gas constant
r	=	radial coordinate (origin at center of sample)
r_0	=	radius of metal sample
T	=	temperature
t	=	time
u	=	velocity
V	=	diffusion velocity
W	=	molecular weight
X	=	mole fraction
Y	=	mass fraction
λ	=	thermal conductivity
ρ	=	density
ω	=	molar production rate

Subscripts

b	=	burning, boiling
f	=	fuel
g	=	gas phase
j, k	=	species index
r	=	radial coordinate
s	=	surface

Received 11 August 2000; revision received 19 December 2000; accepted for publication 20 December 2000.

*Research Associate, Department of Mechanical Engineering, Center for Combustion and Environmental Research, Campus Box 427; abbudmad@spot.colorado.edu. Member AIAA.

†Graduate Student, Department of Mechanical Engineering, Center for Combustion and Environmental Research. Member AIAA.

‡Professor, Department of Mechanical Engineering, Center for Combustion and Environmental Research. Member AIAA.

§Professor, Department of Mechanical Engineering, Center for Combustion and Environmental Research. Associate Fellow AIAA.

Introduction

As a result of the ongoing exploration of Mars and the several missions planned for the future, increased attention has been given to the use of the natural resources of the planet for rocket propellant production and energy generation. Because the atmosphere of Mars consists of approximately 95% carbon dioxide (CO_2), this gas is the resource of choice to be employed for these purposes. Unfortunately, CO_2 is also a final product in most combustion reactions, requiring further processing to extract useful reactants such as carbon monoxide (CO), oxygen (O_2), and hydrocarbons. An exception is the use of CO_2 as an oxidizer reacting directly with metal fuel. Because many metals burn vigorously with CO_2, these may be used as an energy source or as propellants for a research vehicle on the surface of Mars.

Because of its high adiabatic flame temperature, relatively high specific impulse at high oxidizer/fuel ratios, and large heat per unit mass of fuel, as well as its low ignition temperature and low toxicity of the metal and its oxides, magnesium (Mg) has been identified as the most promising metal fuel with CO_2 as oxidizer. Yuasa and Isoda[1] studied ignition and combustion of large Mg disks in CO_2 and showed that Mg had easy ignitability and fast combustion rates in CO_2. They concluded that the combustion products consisted of magnesium oxide (MgO) and CO. Shafirovich and Goldshleger[2] conducted experiments with spherical particles up to 2.5 mm in diameter and found that the burning process was controlled by diffusion and that the particles exhibited pulsating combustion due to superheating of the Mg vapor trapped inside a protective oxide shell. They also proposed a reaction mechanism based on the gas-phase reaction $Mg + CO_2 \rightarrow MgO + CO$ and the heterogeneous reaction $Mg + CO \rightarrow MgO + C$ occurring on the sample surface. Legrand et al.[3] corroborated the experimental findings of Shafirovich and Goldshleger[2] with particles in the 50 μm–2.5 mm range and established the $t_b = Kd^2$ relationship for the burning time t_b of Mg particles with diameter d with $K = 0.5$ s/mm^2.

In all of the preceding studies, with large Mg particles, the burning process is invariably influenced by strong convective currents that accelerate the combustion reaction and shorten the burning times. Although these currents are nearly absent in the burning of small particles, the high emissivity of the flames, rapid reaction, and small length scales make the gathering of any useful information on burning rates and flame structure very difficult. The goal of this investigation is to provide a detailed study of flame structure by taking

advantage of large, free-floating spherical metal samples and their corresponding long burning times available in a weightless environment. The use of reduced gravity is essential to eliminate the intrusive buoyant flows that plague high-temperature metal reactions, to remove the destructive effect of gravity on the shape of molten metal samples, and to study the combustion behavior of metals in the presence of solid oxides undisturbed by natural convection. This work presents the first microgravity experiments conducted with large cylindrical Mg samples burning in CO_2 and CO and a simplified numerical model attempting to explain the experimental observations.

Experimental Apparatus

The apparatus and experimental procedures used in this investigation have been thoroughly described previously[4]; hence, only a brief description will be given here. The ignition source consists of a 1000-W xenon lamp that generates a highly collimated beam with broadband radiation (300–1100 nm). An aspheric lens focuses the beam to provide a 2-MW/m^2 power density on the top surface of the metal specimen. Cylindrical metal samples of 2, 3, and 4 mm diam (with length equal to diameter) are used. The sample is supported by a 0.13-mm-diam, type-*R* thermocouple, whose junction is placed in the center of the specimen. The ends of the thermocouple are attached to diametrically opposite mounting poles, leaving the specimen at the center of the chamber and at the focal length of the aspheric lens. The thermocouple measures the temperature during the heat-up and ignition phases and is eventually destroyed by the flame formed around the sample. This supporting technique allows the formation of a spherically symmetric flame around a free-floating specimen in the absence of gravity. The nearly spherical shape of the sample is achieved after its melting before ignition. For some runs, a type-*C*, tungsten–rhenium thermocouple is used to obtain the inside temperature of the sample and the flame temperature during combustion.

A 4.5-L, stainless steel, cylindrical combustion vessel houses the lens and metal specimen. Optical access for the movie camera and spectrograph is provided through two fused-silica side windows, and a third window is used for sample replacement. Mg specimens (99.95% purity) are burned in a pure CO_2 or pure CO environment (99.6% minimum) at a 1-atm pressure.

A high-speed, 16-mm movie camera provides surface and flame visualization; the images are also used for measurement of burning times. In addition to visible light imaging, time- and space-resolved spectral information of gas-phase reactants and products is obtained with an imaging spectrograph and a 1024-element diode array detector.

The experiment is controlled entirely by a computer, a digital/analog data acquisition board, and an interface code written in graphical programming software. The reduced-gravity experiments were conducted onboard the NASA KC-135 research aircraft in Houston, Texas. Up to 20 s of reduced gravity ($\pm$0.01 g) were available in a single parabolic maneuver. A total of 28 tests were conducted during a one-week series of flights.

Numerical Model

In the case of metal combustion experiments conducted in microgravity, a spherical symmetry during burning and the absence of natural-convection buoyant plumes are nearly achieved. The present experimental effort is complemented by the development of a numerical simulator, DROPLET, to model the spherically symmetric, quasi-steady burning of a metal fuel droplet with full gas-phase chemical kinetics and transport properties calculations. Because of the lack of kinetic and thermophysical data for the heterogeneous reactions of Mg and the absence of a complete condensation mechanism of MgO, the present model does not take into account surface reactions, radiation heat transfer, or complete condensation processes. Only vaporization of Mg from the sample surface is considered (with no heterogeneous surface reactions), and MgO condensation is treated with an Arrhenius-type rate expression for the molar production rate of the liquid, MgO(l) and solid oxide, MgO(s). The condensed products, MgO(l) and MgO(s), are treated like gas-phase species with a low diffusivity.

There are several numerical models already developed for the combustion of aluminum (Al) particles[5–8] that take into account some of the preceding processes not included in the present simulation. Unfortunately, these models can not be used in the case of Mg combustion because knowledge of the kinetic and thermophysical properties of Mg and its oxide is not as extensive as for Al. Thus, the present model is developed to help in the interpretation of the experimental results and to serve as a preliminary effort for further development of a more complete and much needed model of Mg combustion.

Before attempting a Mg–CO_2 flame simulation, preliminary simulations of Mg–O_2 and Mg–air flames are performed because the reaction mechanisms for these systems are better understood. Equilibrium calculations by the NASA-Lewis chemical equilibrium code[9] are performed for all three of the preceding metal-oxidizer combinations to identify the most important species and to obtain the equilibrium temperature.

Mathematical Formulation

The one-dimensional conservation equations describing the quasi-steady burning of a spherical droplet in a quiescent gaseous atmosphere are

$$\frac{1}{r^2}\frac{\partial}{\partial r}\left(r^2\rho u_r\right) = 0 \tag{1}$$

$$\rho u_r C_P \frac{\partial T}{\partial r} = \frac{1}{r^2}\frac{\partial}{\partial r}\left(r^2\lambda\frac{\partial T}{\partial r}\right) - \sum_{k=1}^{k_g}\rho Y_k V_k C_{P,k}\frac{\partial T}{\partial r} - \sum_{k=1}^{k_g} h_k\omega_k W_k \tag{2}$$

$$\rho u_r\frac{\partial Y_k}{\partial r} = -\frac{1}{r^2}\frac{\partial}{\partial r}\left(r^2\rho Y_k V_k\right) + \omega_k W_k \tag{3}$$

The independent variable in these equations is the radial coordinate r. The mass density ρ is calculated from the ideal-gas equation. The model assumes a uniform droplet temperature, and the pressure is considered constant throughout the domain.

The multicomponent transport formulations are used for calculation of all transport properties. The species diffusion velocities are then expressed as

$$V_k = \frac{1}{X_k\bar{W}}\sum_{j=1}^{k_g} W_j D_{kj}\frac{\mathrm{d}X_j}{\mathrm{d}r} - \frac{D_k^T}{\rho Y_k T}\frac{\mathrm{d}T}{\mathrm{d}r} \tag{4}$$

Boundary Conditions

To solve the governing equations described, the following boundary conditions are imposed:

As $r\to\infty$,

$$Y_k = Y_{k,\infty}, \qquad T = T_\infty$$

At $r = r_s$,

$$\rho_s Y_{k,s}(u_r + V_k)_s = \omega_{k,s} W_k \tag{5}$$

$$\lambda_s\left(\frac{\partial T}{\partial r}\right)_s = (\rho u_r)_s H_{fg} \tag{6}$$

$$Y_{f,s} = \frac{W_f}{\bar{W}}\exp\left[-\frac{H_{fg}}{R_f}\left(\frac{1}{T_s} - \frac{1}{T_b}\right)\right] \tag{7}$$

Equation (5) is the species mass balance for the species at the surface, implying that the chemical species flux at the surface is the same as the amount produced or destroyed by the surface chemical

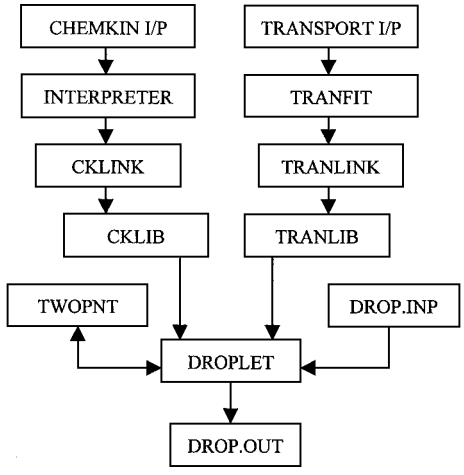

Fig. 1 Flowchart of DROPLET numerical simulator.

reaction. Equation (6) is the surface energy balance, and Eq. (7) is the Clausius–Clapeyron liquid–vapor equilibrium relationship applied to the fuel.

When the preceding equations are solved, it is assumed that there is no reaction at the surface, and so the right-hand side is zero in Eq. (5). Equation (1) can be simplified as

$$r^2 \rho u_r = M_f \tag{8}$$

where the mass flux M_f is a constant. Thus, M_f is conserved throughout the domain. Use of this conserved scalar simplifies other governing equations. Hence, there is no need to solve for the velocity field.

Solution Method

Finite difference approximations for nonuniform mesh spacing are used to solve the resulting system of partial differential equations by forming corresponding algebraic equations. Diffusive terms use central differences with truncation error that is second order in mesh spacing. For better convergence, convective terms use upwind differencing with truncation error that is first order in the mesh spacing. Use of Eq. (8) suggests that the resulting matrix structure is non-symmetric. Because TWOPNT,[10] the boundary value problem solver used by this simulator, needs a block tridiagonal matrix structure, this equation is copied at each grid point. Also, no boundary condition is required for the mass flux far from the particle. The basic solution method is based on a damped modified Newton iteration. A time-stepping algorithm is incorporated to help bring the successive iterations within the domain of convergence for Newton's method.

DROPLET is the simulator written for this specific problem. It uses CHEMKIN[11] and the transport package for kinetics and transport calculations, respectively. The flowchart of the simulator is shown in Fig. 1. The input to CHEMKIN consists of the reaction mechanism and the thermodynamic data. Input to the transport package are the transport property data. The CHEMKIN interpreter and the transport fitting code write respective linking files that can be retrieved by the corresponding libraries, such as CKLIB and TRANLIB. It also uses the boundary value problem solver, TWOPNT, to solve the resulting system of algebraic equations. The input file to DROPLET takes input from the user that consists of the pressure, initial number of grid points, ambient (far-field) conditions, and guessed values of surface and maximum temperatures. The output file written by DROPLET contains the initial guess and the final solution, along with the intermediate solutions found on smaller grids.

Experimental Results

The objective of the present experiments is to characterize the burning behavior of Mg in the presence of CO_2 and CO in a low-gravity environment, as well as to obtain a correlation of burning times with sample size. For this purpose, tests are conducted with cylindrical specimens with 2, 3, and 4 mm diam and length at 1-atm pressure with either pure CO_2 or pure CO. This set of experiments also evaluates the concept of burning a spherical sample in a free-floating configuration in low gravity. The following description of experimental results is based on the temperature measurements, film images, and spectroscopic measurements used as diagnostic tools.

Figure 2 shows a sequence of photographs of the burning of a 3-mm-diam Mg sample in CO_2 in reduced gravity. A nearly

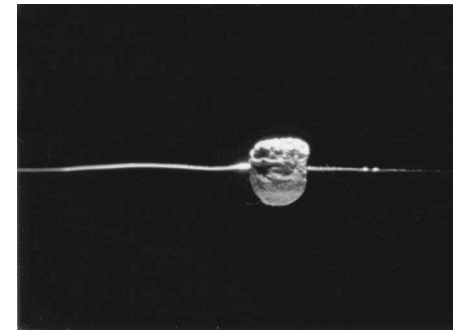

a) Heating and surface oxidation

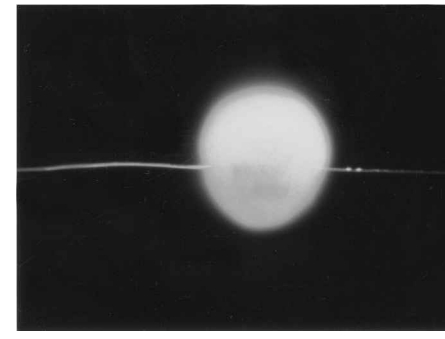

b) Initial flame after ignition (Xe lamp on)

c) Steady-state burning (Xe lamp off)

d) Oxide accumulation around burning specimen

Fig. 2 Sequence of photographs showing the burning of a 3-mm-diam Mg sample in CO_2 at 1 atm in low gravity.

spherical sample is achieved during low gravity after melting and while the specimen is suspended from the thermocouple wire. A smooth surface is not generated due to the oxide film coating formed during the heat-up phase (Fig. 2a). Nonetheless, a nearly spherical flame forms around the sample after ignition, which then immediately melts the thermocouple wire in both sides, permitting the unsupported burning of the free-floating metal. The spherical shape of the surrounding flame is sometimes altered by small convective currents generated by the ubiquitous gravitational jitter experienced during the parabolic trajectory of the airplane.

In the case of Mg in a pure CO_2 atmosphere, ignition occurs at the top of the sample as a result of being heated from above. The ignition occurs near 1100 K. The ignition wave propagates across the sample, ultimately forming a spherical flame around it (Fig. 2b). Steady-state burning is achieved with the visible flame edge anchored at a radius approximately twice the diameter of the specimen (Fig. 2c). The burning sample remains in its central position, which is perturbed only by initial explosions and the gravitational jitter present in the airplane. The explosions are probably a result of the superheating of the metal vapor inside its protective oxide shell. This explosive phenomenon is also observed in $Mg–O_2$ flames[4] and has been reported previously in $Mg–CO_2$ reactions.[12] Several explosions occur during the first few seconds of combustion. Slow, sometimes pulsating burning follows afterward with the increasing accumulation of solid products in an outer shell (Fig. 2d). The sample remains black with some solid white oxide forming in the surface. For most of the metal samples, the end of combustion is accompanied by one final explosion of the metal core that scatters the surface oxide that was formed during the heat-up and burning stages. After a test, very fine particles of MgO(s) in weblike formations are found all around inside the combustion chamber.

The average burning time of the 2-mm samples is 5 s, with burning times of up to 18 s for the 4-mm samples. Figure 3 shows the correlation of burning times with initial sample diameter for the low-gravity experiments along with the results from normal-gravity tests conducted by Legrand et al.[3] with particles in the 50 μm–2.5 mm range. These results correlate well with the $t_b = Kd^2$ expression obtained by Legrand et al.,[3] although the burning times in low-gravity ($K \approx 1$ s/mm^2) are twice as long as the ones obtained in normal gravity ($K \approx 0.5$ s/mm^2). Previous experiments performed by Abbud-Madrid et al.[4] with Mg in pure O_2 showed the same trend in burning times between normal and low gravity. It appears that the slower combustion at low gravity is due to the reduced transport of oxidizer to the metal surface. This behavior is expected from a diffusion-controlled reaction. Intermediate values of burning time are found in samples experiencing the low-to-high-gravity transition during a parabolic maneuver. This is clearly evident in some large samples where the burning time exceeds the low-gravity time available. In these cases, a transition from a spherical flame to an elongated plume is observed as convective currents are generated at larger gravitational values.

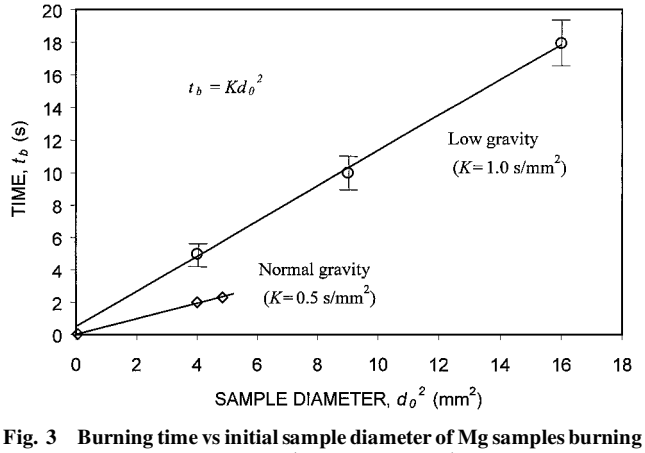

Fig. 3 Burning time vs initial sample diameter of Mg samples burning in CO_2 at 1 atm in low gravity (this investigation) and normal gravity (from Ref. 3).

Although no direct flame temperature measurements are possible with type-*R* thermocouples, spectroscopic records and a few measurements with type-*C* thermocouples indicate a combustion temperature lower than the one observed in $Mg–O_2$ flames.[4] This trend in temperature is in agreement with the adiabatic flame temperature of the $Mg–O_2$ (3398 K) and $Mg–CO_2$ (3174 K) systems obtained by the NASA-Lewis chemical equilibrium code. The spectroscopic measurements show similar features in $Mg–CO_2$ flames as in $Mg–O_2$ flames.[4] The familiar UV and green systems of MgO and Mg appear as the most prominent lines in the gas-phase emission spectra. However, the UV bands of MgO and the UV Mg triplet appear in emission during the complete combustion process in CO_2, whereas the same systems reverse into absorption immediately after ignition in the $Mg–O_2$ flames.[4] No emission bands from CO and CO_2 molecules are detected. These bands may be overshadowed by the strong radiation from Mg and MgO and by the continuum radiation from the oxide particles.

Several tests were conducted with magnesium in pure CO with different sample sizes. The purpose of these experiments was to observe the possible role of the heterogeneous reaction $Mg + CO \rightarrow MgO(s) + C(s)$ in the combustion of Mg with CO_2. In all tests, a dim, slow flame developed around the sample after ignition. The condensed particles of MgO slowly moved outward due to their initial momentum. During combustion, the reacting sample retained the same shape as it had before ignition but with a black coating around it. This phenomenon is shown in Fig. 4 for a 4-mm-Mg sample burning in CO in low gravity. An electron microprobe (EMP) analysis of the black layer around the reacted sample is shown in Fig. 5. The analysis reveals a high carbon content in the thin outer edge of the sample. Because the thickness of this layer is of just a few micrometers, close to the resolution limit of the EMP, it is not possible to determine precisely the nature of the carbon-containing

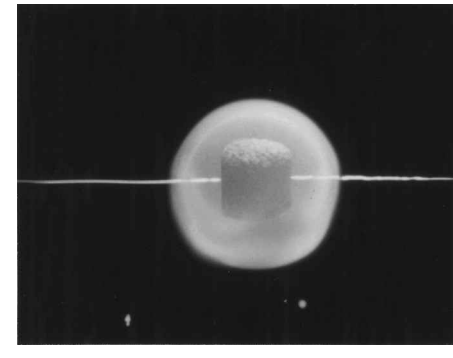

Fig. 4 Photograph of 4-mm-diam-Mg sample burning in CO at 1 atm in low gravity (Xe lamp on).

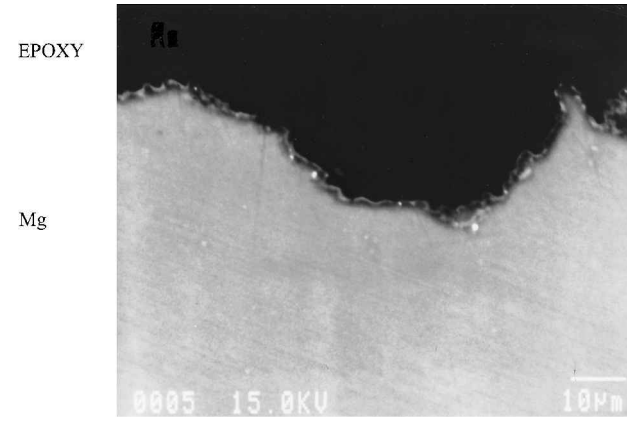

Fig. 5 Electron microprobe photograph of the outer edge of a Mg sample burned in CO at 1 atm in low gravity: the upper black region comes from the epoxy surrounding the sample, the lower bright section shows unreacted Mg, and the thin black layer on the edge of the sample corresponds to a high-carbon content compound [possibly C(s) or Mg_2C_3].

species. As proposed by Goldshleger and Shafirovich[13] in thermogravimetric studies of Mg particles burning in CO_2, carbon may be in its free solid state, C(s), or in the Mg_2C_3 carbide. In all cases of Mg burning in pure CO, it was observed that the reaction continued while the external radiation from the lamp was present, but immediately stopped after the lamp was turned off. From the preceding results, it is concluded that continuous reaction of Mg with pure CO is only possible as long as Mg vapor is continuously extruded through the increasingly thicker carbon coating. This situation requires an isothermal CO environment at a temperature above the ignition temperature.

For all of the cases of Mg combustion described, note that no direct comparison is possible with normal gravity tests with the same experimental setup. At normal gravity, the suspended sample collapses during melting and ignition, forming an elongated flame as it reacts, and eventually extinguishes due to heat losses to the surface below.

Numerical Model Predictions

As explained in the "Numerical Model" section, numerical simulations are first conducted for the Mg–O_2 and Mg–air systems for which the reaction mechanisms are better understood. The reactions in the Mg–O_2 system are then used in the Mg–CO_2 simulation along with the reactions of Mg with CO_2 and CO, as well as all reactions of carbon-containing species with O_2 and O. For all three metal-oxidizer systems mentioned, equilibrium calculations are performed with the NASA-Lewis chemical equilibrium code[9] to identify the most important species and to obtain the equilibrium temperature. For each of the three systems, it is necessary to include all three phases of MgO (gas, liquid, and solid) to obtain a realistic equilibrium temperature as observed in experiments. Including the gas- and liquid-phase species, MgO and MgO(l), as the only oxide products results in unrealistically low temperatures and species concentrations due to the absence of the large heat release experienced from the complete gas-to-solid condensation process. Hence, both the gas-to-liquid and liquid-to-solid condensation mechanisms must be considered for an accurate description of the Mg combustion process.

Mg–O_2 Flame Structure

In the case of Mg–O_2, the equilibrium calculations are performed with 1 mole of gaseous Mg at 1366 K and 1 mole of O_2 at 300 K as the initial conditions. The equilibrium temperature under adiabatic conditions is 3398 K and all three phases of MgO are present at this temperature. The numerical simulation of the Mg–O_2 flame structure uses the following reaction mechanism.

Reaction 1:

$$Mg + O_2 = MgO + O$$

Reaction 2:

$$Mg + O + M = MgO + M$$

Reaction 3:

$$MgO = MgO(l)$$

Reaction 4:

$$MgO(l) = MgO(s)$$

Reaction 5:

$$2O + M = O_2 + M$$

Reactions 1 and 2 and their corresponding rate constants are determined from previous studies.[14] The symbol M represents the presence of a third body. The molar production rate of MgO(l) in reaction 3 is obtained from the Arrhenius-type rate expression[15] of the condensation rate for the formation of drops of the critical radius (condensation nuclei) arising in a unit volume during a unit time.

Table 1 Reaction Mechanism for Mg–O_2[a]

Reaction	Reaction no.	A	β	E_A	Reference
$Mg + O_2 = MgO + O$	1	4.44E+12	0.5	30500.0	14
$Mg + O + M = MgO + M$	2	1.90E+14	0.5	0.0	14
$MgO = MgO(l)$	3	6.11E+11	−2.0	17268.6	15
$MgO(l) = MgO(s)$	4	1.00E+15	0.0	0.0	——
$2O + M = O_2 + M$	5	1.89E+13	0.0	−1788.0	16

[a]Rate coefficients are in the form $K = A^* T^{\beta} \exp(-E_A/RT)$. Units of A are in moles, centimeters, seconds, kelvin, and units of E_A are in calories per mole.

Because of the lack of a similar rate expression for the liquid-to-solid phase transition, a high value of the preexponential factor is used to simulate the condensation process of reaction 4. This parameter is adjusted until a physically acceptable temperature profile is achieved. The condensed products are treated as gas-phase species with very low diffusivity. This is achieved by using a large value of the Lennard–Jones collision diameter in the transport property input. In the present simulations a Lennard–Jones collision diameter of 10 Å is chosen because is of the order of magnitude of the critical radius for condensation (3 Å) of MgO under the given conditions and small enough to avoid the treatment of a condensed phase. This value is used as a collision diameter for both MgO(l) and MgO(s). The rate constants for reactions 1–5 are shown in Table 1 (see also Ref. 16).

Figure 6 shows the flame structure of a 2-mm-diam-Mg droplet burning in pure O_2 at 1-atm pressure and 300-K temperature. Magnesium vapor diffuses out from the particle surface toward the counterdiffusing O_2. The surface temperature is only a few degrees below the boiling point of Mg (1366 K). The temperature profile rises with a very steep gradient near the surface to a short plateau region, where a maximum temperature of 3220 K is reached. After the complete consumption of the Mg vapor, the slope of the temperature profile starts decreasing at a faster rate. The predicted maximum temperature of 3220 K is slightly lower than the maximum equilibrium temperature of 3398 K, that is, the vaporization–decomposition point of MgO under these conditions. This difference in maximum temperature values may be attributed to the lack of an accurate condensation model, which may also be responsible for the absence of a large concentration of MgO(l) in the plateau region where the temperature exceeds the melting point of MgO (3105 K) and where the liquid oxide is the dominant species. The high preexponential factor used to simulate the liquid-to-solid phase change is insensitive to temperature and, thus, unable to simulate the rise of MgO(l) in the temperature plateau region. Hence, only a very small amount of MgO(l) is obtained in the present calculations.

The gaseous oxide profile, MgO, shows a peak at the highest temperature and then rapidly decreases. As a result of the high flame temperature, a large amount of atomic oxygen O is also found in the plateau region of the temperature profile. The simulation also shows the diffusion of molecular oxygen O_2 to the particle surface. Its significant concentration at the surface indicates that heterogeneous reactions may play an important role at the surface of the sample.

As mentioned before, the liquid and solid oxides are treated as gas-phase species with low diffusivity by using a Lennard–Jones collision diameter of 10 Å, a value of the same order of magnitude as the critical radius of condensation. To test the effectiveness of this approach, a collision diameter of 25 Å was used under the same conditions as in the original simulation. Under this higher collision diameter, the burning rate decreases by a factor of two and, hence, the burning time increases by the same magnitude. Therefore, it appears that increasing the agglomeration of condensed products around the reaction zone results in increased hindrance to the transport of the gaseous oxidizer. However, because the estimate of burning times and, hence, the corresponding d^n law, are strongly dependent on the assumed value of the collision diameter, no direct comparison with experimental burning times can be done without the inclusion of complete condensation and agglomeration mechanisms.

Nevertheless, as will be seen in the following sections, comparisons can be done between burning rates obtained by simulation for the Mg–O_2, Mg–air, and Mg–CO_2 systems.

Mg–Air Flame Structure

In the case of the Mg–air system, the equilibrium calculations are performed with 1 mole of gaseous Mg at 1366 K and 1 mole of air at 300 K as the initial conditions. The equilibrium temperature under adiabatic conditions is 3220 K with all three phases of MgO present at this temperature. For the numerical simulation of the Mg–air flame structure, nitrogen (N_2) is added (79% by volume) to the oxidizer to simulate the burning of Mg in air. The GRI-Mech™ 2.11 mechanism[17] is used to add the nitrogen chemistry to the Mg–O_2 mechanism. Other product species such as Mg_3N_2 and MgN are neglected in the present analysis due to the lack of kinetics and transport property information. The condensation of MgO into MgO(l) and MgO(s) is treated in the same manner as in the Mg–O_2 case. The reaction mechanism and rate constants for the Mg–air system are shown in Table 2, which shows reactions 1–10.

Figure 7 shows the flame structure of a 2-mm-diam-Mg droplet burning in air at 1-atm pressure and 300-K temperature. As in the Mg–O_2 flame, the temperature profile rises sharply near the droplet surface. The maximum temperature in this case, however, is 3143 K, which is lower than in the Mg–O_2 system due to the presence of N_2. This predicted maximum temperature of the Mg–air flame is also lower than the adiabatic flame temperature obtained in the equilibrium calculations (3220 K) due to the lack of an accurate condensation model, which is also responsible for the absence of any significant concentration of MgO(l) in the temperature plateau region. The predicted burning rate is 1.5 times smaller than that obtained in the Mg–O_2 simulation. Also, an increase in the Lennard–Jones collision diameter to 25 Å decreases the burning rate by a factor of two, which is in excellent quantitative agreement with the trend obtained in the simulation of Mg burning in pure oxygen.

Table 2 Reaction Mechanism for Mg–Air[a]

Reaction	Reaction no.	A	β	E_A	Reference
$Mg+O_2=MgO+O$	1	4.44E+12	0.5	30500.0	14
$Mg+O+M=MgO+M$	2	1.90E+14	0.5	0.0	14
$MgO=MgO(l)$	3	6.11E+11	−2.0	17268.6	15
$MgO(l)=MgO(s)$	4	1.00E+15	0.0	0.0	——
$2O+M=O_2+M$	5	1.89E+13	0.0	−1788.0	16
$N+NO=N_2+O$	6	3.50E+13	0.0	330.0	17
$N+O_2=NO+O$	7	2.65E+12	0.0	6400.0	17
$N_2O+O=N_2+O_2$	8	1.40E+12	0.0	10810.0	17
$N_2O+O=2NO$	9	2.90E+13	0.0	23150.0	17
$NO_2+O=NO+O_2$	10	3.90E+12	0.0	−240.0	17

[a]Rate coefficients are in the form $K=A^*T^{\beta}\exp(-E_A/RT)$. Units of A are in moles, centimeters, seconds, kelvin, and units of E_A are in calories per mole.

Mg–CO_2 Flame Structure

For the Mg–CO_2 system, an equilibrium calculation performed with 1 mole of gaseous Mg at 1366 K and 1 mole of CO_2 at 1000 K gives an equilibrium temperature under adiabatic conditions of 3174 K with all three phases of MgO present at this temperature. For the numerical simulation of the Mg–CO_2 flame structure, the reaction mechanism proposed by Shafirovich and Goldshleger[2] (described in the "Introduction") is used for the reactions of Mg with CO_2 and CO.

Reaction 11:

$$Mg + CO_2 = MgO + CO$$

Reaction 12:

$$Mg + CO = MgO + C$$

The elementary steps and rate constants for reactions of carbon-containing species with O_2 and O are taken from the GRI-Mech 2.11 mechanism[17] and are shown in Table 3 along with all of the Mg–O_2 and Mg–CO_2 reactions, including reactions 13–15. Because the rate constants for reactions 11 and 12 are not well known, these constants are obtained for the present study from a sensitivity analysis and its comparison with experimental results. Species such as $MgCO_3$,

Table 3 Reaction Mechanism for Mg–CO_2[a]

Reaction	Reaction no.	A	β	E_A	Reference
$Mg+CO_2=MgO+CO$	11	2.00E+14	0.0	34847.0	2
$Mg+CO=MgO+C$	12	2.00E+11	0.0	30000.0	2
$Mg+O_2=MgO+O$	1	4.44E+12	0.5	30500.0	14
$Mg+O+M=MgO+M$	2	1.90E+14	0.5	0.0	14
$MgO=MgO(l)$	3	6.11E+11	−2.0	17268.6	15
$MgO(l)=MgO(s)$	4	1.00E+15	0.0	0.0	——
$2O+M=O_2+M$	5	1.89E+13	0.0	−1788.0	16
$CO+O+M=CO_2+M$	13	6.02E+14	0.0	3000.0	17
$CO+O_2=CO_2+O$	14	2.50E+12	0.0	47800.0	17
$C+O_2=CO+O$	15	5.80E+13	0.0	576.0	17

[a]Rate coefficients are in the form $K=A^*T^{\beta}\exp(-E_A/RT)$. Units of A are in moles, centimeters, seconds, kelvin, and units of E_A are in calories per mole.

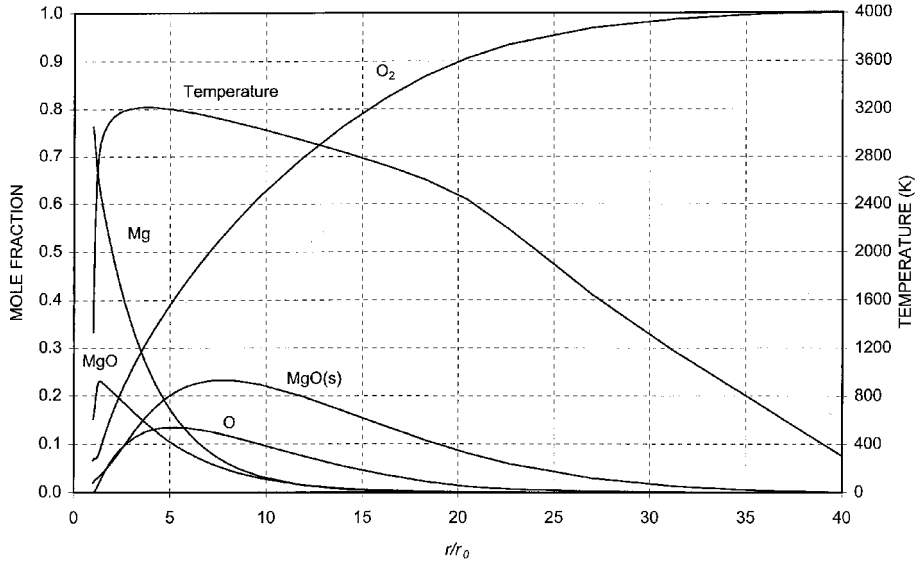

Fig. 6 Flame structure of 2-mm-diam-Mg droplet burning in O_2 obtained with DROPLET numerical simulator.

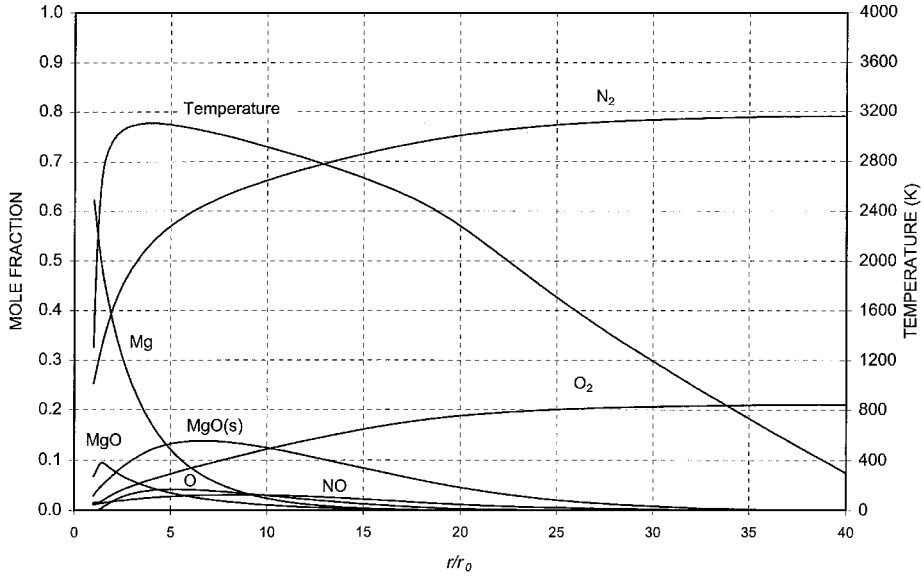

Fig. 7 Flame structure of 2-mm-diam-Mg droplet burning in air obtained with DROPLET numerical simulator.

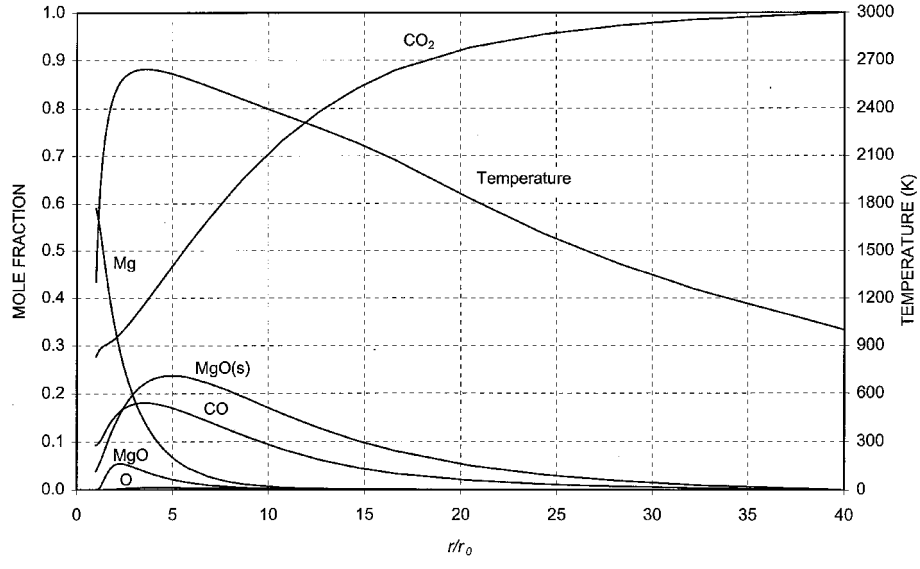

Fig. 8 Flame structure of 2-mm-diam-Mg droplet burning in CO_2 obtained with DROPLET numerical simulator.

MgC, and Mg_2C_3, predicted by the equilibrium calculations, are neglected in the present analysis due to the lack of kinetics information. As described in the "Experimental Results" section, thermogravimetric studies[13] suggest that some of these carbon-containing species may form on the surface of the particle. Condensation processes are treated in the same manner as in the Mg–O_2 and Mg–air cases.

The flame structure of a 2-mm-diam-Mg droplet burning in a pure CO_2 atmosphere at 1-atm pressure is shown in Fig. 8. In this case the oxidizer ambient temperature is 1000 K because no convergence is obtained in the simulation for lower temperatures. This numerical result is in agreement with experimental studies[2] where the Mg sample is ignited by slowly heating the CO_2 gas around it. In these tests, no burning is obtained for ambient temperatures below 985 K. Under the experimental conditions used in the present investigation, the burning of the Mg sample under CO_2 ambient temperatures as low as 300 K is possible because enough radiant energy is provided to the sample to induce its ignition and subsequent burning before the energy source is turned off. The maximum combustion temperature predicted by the simulation is 2645 K, which is lower than the equilibrium temperature of 3174 K for CO_2 at an ambient temperature of 1000 K. The cause of this discrepancy in maximum temperature values follows the same reasoning as in the Mg–O_2 and Mg–air cases.

The reaction zone observed in Fig. 8 is narrower than in the Mg–O_2 and Mg–air simulations, suggesting a slower molecular diffusion process in the case of CO_2 as the oxidizer. This result is in qualitative agreement with the experiments where longer burning times are observed in Mg–CO_2 flames. The predicted burning rate is slightly lower than the rate obtained in the Mg–air simulation.

Conclusions

This investigation studies the burning behavior and flame structure of Mg in a CO_2 atmosphere to assess the feasibility of using metal–CO_2 reactions as an in situ resource utilization technology for rocket propulsion and energy generation on other planets. An experimental technique consisting of igniting suspended metal samples in reduced gravity is used to generate free-floating, burning bulk metal samples exhibiting a spherically symmetric flame. In this way, spherical flames are obtained during steady-state burning of the metal sample with increasing metal-oxide accumulation in an outer shell. Burning times twice as long as in normal gravity and five times longer than in Mg–O_2 flames are observed, revealing a diffusion-controlled reaction. The burning time is proportional

to the square of the metal sample diameter. In tests conducted with pure CO, combustion is not possible without constant heating of the sample. It appears that surface reactions dominate in this case leaving behind a thick carbon coating around the molten Mg sample.

Because the burning times of the larger samples in CO_2 are in the order of the low-gravity time available in each parabolic maneuver of the aircraft, in some cases it was necessary to start the heating of the sample in the high-gravity portion of the trajectory preceding the weightlessness period. In these cases, residual convective currents affected the flame shape and the burning rate. The same distorting influence was observed when the burning extended into the low-to-high gravity transition. In addition, it was found that free-floating samples burning in low gravity are very sensitive to gravitational jitter. The spherical shape of the flame tends to be distorted, and the sample changes location in the direction of the gravity level experienced during the flight. Undoubtedly, this experiment could benefit greatly from the long-duration microgravity environment provided by orbiting spacecraft.

A one-dimensional, spherically symmetric, quasi-steady model is used to simulate the burning behavior of Mg in O_2, air, and CO_2. The flame structure predicted by the model shows a temperature profile with a short plateau region at the highest temperature of the flame. It is within this region that the vaporization–dissociation of MgO takes place, acting as an enthalpy sink. Condensation of MgO to MgO(l) and MgO(s) follows thereafter as it diffuses away from the flame. The maximum temperature obtained from the model is lower than that predicted by the equilibrium calculations, and the high concentration of MgO(l) expected in the temperature plateau region is absent from the simulation results. Both effects are due to the lack of accurate information on the rates of liquid-to-solid condensation of the metal oxide.

In accordance with the experiments, the overall burning process appears to be diffusion controlled in all of the cases. The burning rate and the maximum temperature in a CO_2 atmosphere are lower than in O_2 or air. For Mg burning in CO_2, an ambient temperature of 1000 K is necessary for convergence of the simulation, which agrees with experimental observations of samples ignited and burned by slow heating of the surrounding oxidizer.

At the present time, this preliminary model does not give a complete picture of the metal-oxidizer reaction because not all of the relevant physical and chemical mechanisms are considered. Product condensation and agglomeration, radiation heat loss, and heterogeneous surface reactions are just some of the important mechanisms that should be included in the model to provide an accurate representation of the burning process. In addition, there is also a lack of information in the literature on reaction rates of the most basic elementary reactions. Nevertheless, although preliminary, the model provides a qualitative description of the flame structure that helps to visualize the complex phenomenon of metal combustion.

Acknowledgments

This work is supported by NASA under Grant NASA-NAG3-2220. The authors gratefully acknowledge the help of Pierre Omaly (visiting student from the Centre National de la Recherche Scientifique in Orléans, France) during the KC-135 flights, the technical supervision of Robert Friedman from the NASA John H. Glenn Research Center at Lewis Field, and the many helpful discussions with Robert Kee from the Colorado School of Mines.

References

[1] Yuasa, S., and Isoda, H., "Ignition and Combustion of Metals in a Carbon Dioxide Stream," *Proceedings of the Twenty-Second International Symposium on Combustion*, Combustion Inst., Pittsburgh, PA, 1988, pp. 1635–1641.

[2] Shafirovich, E. Ya., and Goldshleger, U. I., "Combustion of Magnesium Particles in CO_2/CO Mixtures," *Combustion, Science, and Technology*, Vol. 84, Nos. 1–6, 1992, pp. 33–43.

[3] Legrand, B., Shafirovich, E. Ya., Marion, M., Chauveau, C., and Gökalp, I., "Ignition and Combustion of Levitated Magnesium Particles in Carbon Dioxide," *Proceedings of the Twenty-Seventh International Symposium on Combustion*, Combustion Inst., Pittsburgh, PA, 1998, pp. 2413–2419.

[4] Abbud-Madrid, A., Branch, M. C., and Daily, J. W., "Ignition and Combustion of Bulk Titanium and Magnesium at Normal and Reduced Gravity," *Proceedings of the Twenty-Sixth International Symposium on Combustion*, Combustion Inst., Pittsburgh, PA, 1996, pp. 1929–1936.

[5] Law, C. K., "A Simplified Theoretical Model for the Vapor-Phase Combustion of Metal Particles," *Combustion, Science, and Technology*, Vol. 7, No. 5, 1973, pp. 197–212.

[6] King, M. K., "Modeling of Single Particle Aluminum Combustion in CO_2–N_2 Atmospheres," *Proceedings of the Seventeenth International Symposium on Combustion*, Combustion Inst., Pittsburgh, PA, 1979, pp. 1317–1328.

[7] Brooks, K. P., and Beckstead, M. W., "Dynamics of Aluminum Combustion," *Journal of Propulsion and Power*, Vol. 11, No. 4, 1995, pp. 769–780.

[8] Bucher, P., Yetter, R. A., Dryer, F. L., Parr, T. P., Hanson-Parr, D. M., "PLIF Species and Ratiometric Temperature Measurements of Aluminum Particle Combustion in O_2, CO_2 and N_2O oxidizers, and Comparison with Model Calculations," *Proceedings of the Twenty-Seventh International Symposium on Combustion*, Combustion Inst., Pittsburgh, PA, 1998, pp. 2421–2429.

[9] McBride, B. J., and Gordon, S., "Computer Program for Calculation of Complex Chemical Equilibrium Compositions and Applications," NASA John H. Glenn Research Center at Lewis Field, Reference Publ. 1311, Cleveland, OH, 1996.

[10] Grcar, J. F., "The Twopnt Program for Boundary Value Problems," Sandia National Labs., Rept. SAND91-8230, Livermore, CA, 1992.

[11] Kee, R. J., Miller, J. A., and Jefferson, T. H., "CHEMKIN: A General-Purpose, Problem-Independent, Transportable, Fortran Chemical Kinetics Code Package," Sandia National Labs., Rept. SAND80-8003, Livermore, CA, 1980.

[12] Shafirovich, E. Ya., and Goldshleger, U. I., "The Superheat Phenomenon in the Combustion of Magnesium Particles," *Combustion and Flame*, Vol. 88, Nos. 3–4, 1992, pp. 425–432.

[13] Goldshleger, U. I., and Shafirovich, E. Ya., "Combustion Regimes of Magnesium in Carbon Oxides. 1. Combustion in CO_2," *Combustion, Explosion, and Shock Waves*, Vol. 35, No. 6, 1999, pp. 637–644.

[14] Mellor, A. M., Wittig, S. L. K., and Whitacre, R. F., "Spectrometric Study of Shock-Heated Mg/MgO Particle Dispersions," *Combustion, Science, and Technology*, Vol. 4, No. 1, 1971, pp. 31–36.

[15] Pilyugin, N. N., "Nonequilibrium Magnesium-Related Processes in the Wake Behind a Model Moving with Hypersonic Speed in Air," *Combustion, Explosion, and Shock Waves*, Vol. 36, No. 3, 2000, pp. 349–357.

[16] Tsang, W., and Hampson, R. F., "Chemical Kinetic Database for Combustion Chemistry," *Journal of Physical and Chemical Reference Data*, Vol. 15, No. 3, 1986, pp. 1087–1279.

[17] Bowman, C. T., Hanson, R. K., Gardinger, W. C., Jr., Lissianski, V., Frenklach, M., Goldenberg, M., and Smith, G. P., "GRI-Mech—An Optimized Detailed Chemical Reaction Mechanism for Methane Combustion and NO Formation and Reburning," Gas Research Inst., Rept. 97-0020, Des Plaines, IL, 1997.